J. Austral. Math. Soc. Ser. B 25 (1983), 64–83

THE GENERATION OF SURFACE WAVES BY AN INTENSE CYCLONE

F. VIERA and V. T. BUCHWALD[1]

(Received 4 October 1982; revised 2 December 1982)

Abstract

Assuming a travelling oscillating pressure source model, this paper sets out to investigate the observation of surface gravity waves generated by a cyclone moving with constant speed v. It is shown that when the source frequency is near the critical resonant value $g/4v$, large amplitude waves may be generated. There is some agreement with observations of waves from cyclone Pam of February, 1974.

I. Introduction

In February 1974, the tropical cyclone Pam travelled parallel to the east coast of Australia for about three days at a distance of about 650 km, at a speed of about 20 km/h and generated large amplitude waves of period of about 7 seconds.

Isobars observed at 11 *a.m.* on the 6th of February, are shown in Figure 1a, and the estimated path of the storm centre is shown in Figure 1b. Table 1 gives data obtained by the Maritime Services Board of N.S.W. from a waverider buoy 2 km off-shore at Botany Bay (near Sydney). On the 6th of February between 5 *a.m.* and 3 *p.m.*, an abrupt change was observed in the energy density and wave height. Large waves were then recorded for about two days until the evening of the 8th of February.

In order to seek an explanation of the observations, we model the cyclone by a travelling oscillating point pressure source which generates surface waves as it moves with constant speed. Although this assumption cannot describe the wave generation mechanism in the storm region itself nor the overall effect of a frequency spectrum, it will be shown to be useful in the study of waves at long distances from the storm centre.

[1]School of Mathematics, University of New South Wales, Kensington, N.S.W. 2033.

The generation of surface gravity waves in two dimensions by travelling oscillating pressure distributions has been discussed by Lighthill [6], among others. For a fixed value of source frequency, the dispersion relation of such waves is a curve in wavenumber space. Points of inflexion on such curves generate caustic solutions which give rise to waves of relatively large amplitude. These waves are observed in a direction from the source which is normal to the curve at that point.

However, to explain the large waves generated by the cyclone, one should also look for the possibility of resonance. It can be shown that the group velocity of the waves matches the source speed when the product of the source speed and frequency equals one quarter of the gravitational acceleration g. At this critical point there is a build-up of energy around the source and large amplitudes may ensue. For cyclone Pam, the observed wave amplitudes and periods are in accord with those predicted by this mechanism.

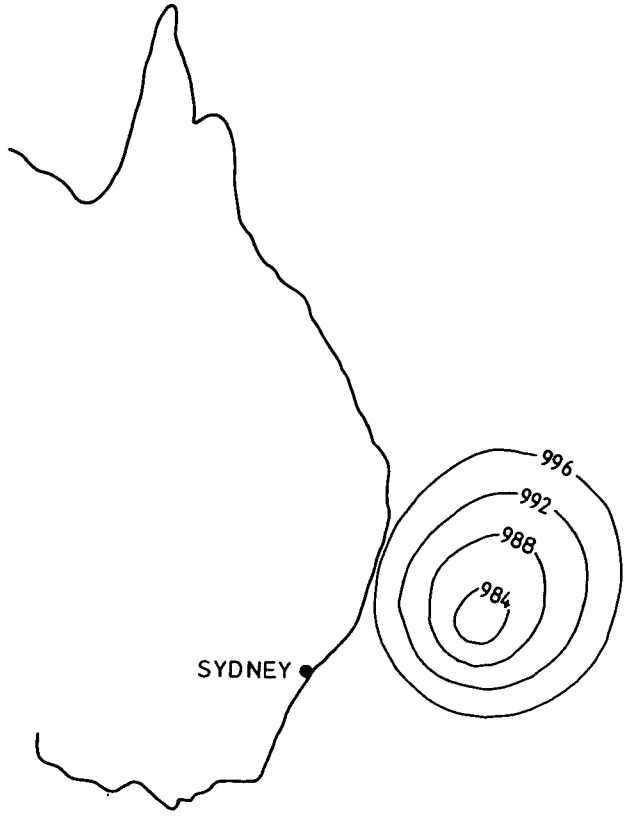

Figure 1a. Isobars from cyclone Pam, observed at 11 *a.m.* on the 6th of February, 1974 (day 37). Values shown are in millibars

https://doi.org/10.1017/S033427000000391X Published online by Cambridge University Press

In order to formulate the problem, take Cartesian coordinates (x', y', z') with the z'-axis pointing upwards such that the pressure source is at rest and the fluid moves in the positive x'-direction with speed v relative to this frame. Define non-dimensional coordinates by

$$(x, y, z) = (x', y', z')g/v^2, \qquad t = t'g/v, \tag{1}$$

where t' is the time, and let $\phi(x, y, z, t) = \phi'(x', y', z', t')/v$ where ϕ' is the velocity potential. If $\eta(x, y, t)$ is the displacement of the free surface from equilibrium, the linearized wave equations in deep water reduce to

$$\frac{\partial^2\phi}{\partial x^2} + \frac{\partial^2\phi}{\partial y^2} + \frac{\partial^2\phi}{\partial z^2} = 0, \qquad [-\infty < x, y < \infty, -\infty < z < 0], \tag{2}$$

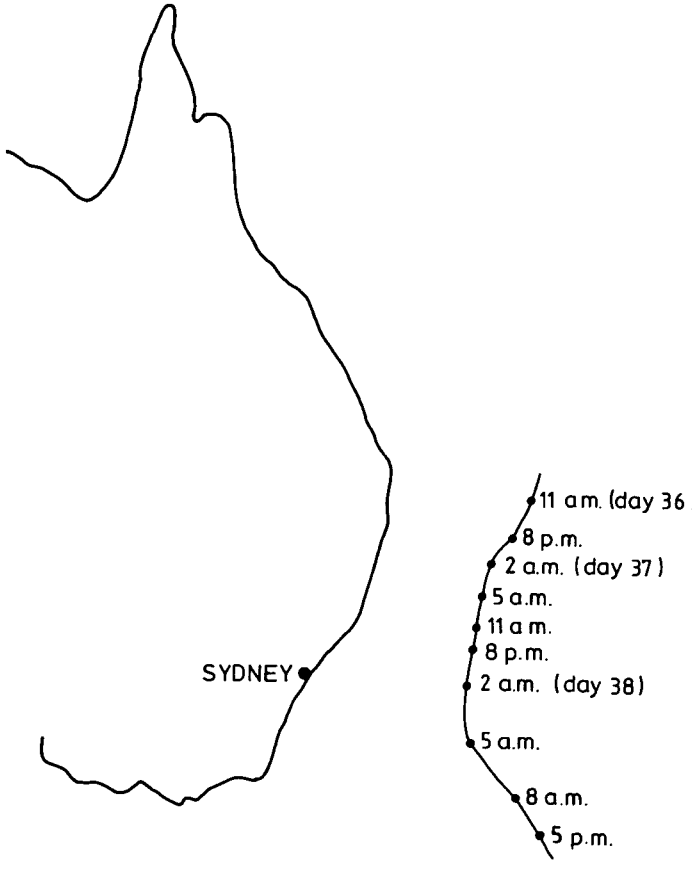

Figure 1b. Estimated positions of the centre of cyclone Pam relative to Sydney. Day 36 is the 5th of February, 1974.

https://doi.org/10.1017/S033427000000391X Published online by Cambridge University Press

$$\left.\begin{aligned} \frac{\partial\phi}{\partial t} + \frac{\partial\phi}{\partial x} + \eta &= -\frac{p}{\rho g}, \\ \frac{\partial\eta}{\partial t} + \frac{\partial\eta}{\partial x} &= \frac{\partial\phi}{\partial z}, \end{aligned}\right\} \quad \text{at } z = 0, \tag{3}$$

and

$$\lim_{z \to -\infty} \partial\phi/\partial z = 0, \tag{4}$$

where ρ is the constant density of the fluid. The applied pressure is assumed to take the circular symmetric form

$$p(x, y, t) = p_0\delta(x)\delta(y)\exp(-i\sigma_0 t), \tag{5}$$

where p_0 is constant, $\delta(x)$ is the Dirac delta-function and $\sigma_0 = v\omega_0/g$ where ω_0 is the dimensional source frequency.

TABLE 1. Wave data from a waverider buoy located 2 km off-shore outside Botany Bay. Day 36 corresponds to the 5th of February, 1974. The cyclone is estimated to be due East of Sydney at 2.00 *a.m.* on day 38.

Day	Time of Day	Period (sec)	Energy Density (m^2/sec)	RMS Wave Height (m)	Maximum Wave Height (m)
36	14.53	6.67	0.169	1.05	2.94
36	20.56	6.72	0.184	1.10	2.90
37	2.56	7.70	0.221	1.26	2.75
37	8.52	8.52	0.297	1.45	3.91
37	15.03	7.41	0.766	2.25	5.01
37	18.00	7.19	0.855	2.43	5.23
37	21.10	7.14	1.285	3.00	7.08
38	0.06	7.52	1.410	3.16	7.02
38	3.05	7.58	1.587	3.40	7.17
38	6.04	7.20	1.410	3.11	8 15
38	9.00	7.24	1.388	3.14	6.54
38	11.57	6.97	1.027	2.66	6.37
38	15.03	6.62	0.876	2.49	5.83
38	18.00	6.26	0.700	2.21	5.05
38	21.10	6.96	0.797	2.41	5.29
39	0.06	7.13	0.816	2.46	5.91
39	3.05	7.53	0.962	2.67	7.56
39	6.04	7.23	0.836	2.39	5.59
39	9.00	8.03	1.018	2.76	5.85
39	11.57	7.25	0.739	2.29	5.31
39	15.03	7.71	0.798	2.40	5.46
39	18.00	7.56	0.769	2.31	4.89
39	21.10	7.34	0.509	1.95	4.14
40	3.00	7.43	0.568	1.98	4.57
40	9.00	7.09	0.444	1.78	3.90

https://doi.org/10.1017/S033427000000391X Published online by Cambridge University Press

The model in (3) and (5) is not intended to suggest that a fluctuating pressure source is the actual mechanism for the generation of the observed waves. The waves are generated, of course, by the high rotary winds near the stormcentre, the details of which are not our concern. What is important is that large wave generation is confined to the storm region so that an observer located well outside the storm will see waves emerging which are somehow generated within that region. The wave properties that are investigated in this paper are largely independent of the source mechanism, and we may as well, therefore, assume the simplest possible source, which is a fluctuating pressure distribution. Note, though, that the actual distribution of waves radiated from the storm is probably not circularly symmetric and the theory in this paper would then need to be amended to take asymmetry into account. Nevertheless, the assumed symmetric model is a useful starting point for understanding the geometry of the propagating waves. An actual cyclone would, of course, also have a continuous frequency distribution, but the single frequency model used here is useful in seeking those frequencies for which the distant observer is likely to see large waves.

2. Asymptotic representation of $\eta(x, y, t)$

Define the double Fourier transform by

$$A(\alpha, \beta) = \frac{1}{2\pi}\int_{-\infty}^{\infty}\int_{-\infty}^{\infty} a(x, y)e^{-i(\alpha x+\beta y)}dx\,dy, \tag{6}$$

and assume that ϕ and η have an implicit harmonic dependence of the form $\exp(-i\sigma_0 t)$. Application of (6) to (2), (3) and (4) with (5) and use of Fourier's inversion theorem yields the solution

$$\eta(x, y, t) = \frac{-p_0 e^{-i\sigma_0 t}}{4\pi^2\rho g}\int_{-\infty}^{\infty}\int_{-\infty}^{\infty}\frac{(\alpha^2+\beta^2)^{1/2}e^{i(\alpha x+\beta y)}d\alpha\,d\beta}{G(\alpha, \beta, \sigma_0)}, \tag{7}$$

where

$$G(\alpha, \beta, \sigma_0) = (\alpha^2+\beta^2)^{1/2} - (\alpha-\sigma_0)^2. \tag{8}$$

Note that $G = 0$ is the wavenumber curve, shown in Figure 2 for various values of the source frequency σ_0. Also shown in Figure 2 is the critical point P at which the wave group velocity matches the source speed v.

Crapper [4], following Lighthill [5], obtained asymptotic expansions of the wave amplitude (7) for the special case $\sigma_0 = 0$, observed along particular directions $\mathbf{r} = (x, y) = r(\cos\theta, \sin\theta)$, where $r = (x^2+y^2)^{1/2}$. The method consists of defining a new system of coordinates $(\bar{\alpha}, \bar{\beta})$ by rotating the original system (α, β)

https://doi.org/10.1017/S033427000000391X Published online by Cambridge University Press

through an angle θ, and then integrating asymptotically using residue theory and the method of stationary phase.

It is easy to generalize the method to the case of arbitrary σ_0, and in fact, at normal points of the wavenumber curve at which the curvature κ is not zero, it was found that

$$\eta \sim \frac{-ip_0 e^{-i\sigma_0 t}}{2\pi\rho g}\left(\frac{2\pi}{r}\right)^{1/2} \sum_m \frac{\left(\alpha_m^2 + \beta_m^2\right)^{1/2}}{\left(\partial G/\partial\bar{\alpha}\right)_m |\kappa|^{1/2}} \exp i\left(\alpha_m x + \beta_m y + \frac{1}{4}\pi \operatorname{sgn}\kappa\right), \tag{9}$$

as $r \to \infty$. The sum is over all points (α_m, β_m) on the curve $G = 0$ such that its normal is parallel to the radius vector $\mathbf{r}$,

$$\bar{\alpha} = \alpha\cos\theta + \beta\sin\theta, \qquad \bar{\beta} = -\alpha\sin\theta + \beta\cos\theta, \tag{10}$$

are the new coordinates in the rotated wavenumber plane,

$$\partial G/\partial\bar{\alpha} = |\nabla G| = \left(G_\alpha^2 + G_\beta^2\right)^{1/2}, \tag{11}$$

and the curvature

$$\kappa = \left(2G_{\alpha\beta}G_\alpha G_\beta - G_\alpha^2 G_{\beta\beta} - G_\beta^2 G_{\alpha\alpha}\right)\left(G_\alpha^2 + G_\beta^2\right)^{-3/2}, \tag{12}$$

where the subscripts denote partial differentiation.

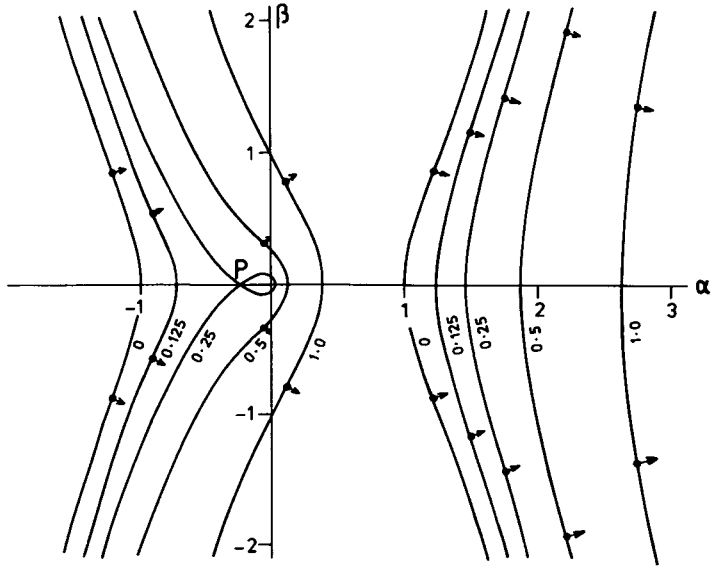

Figure 2. Wavenumber curves $G = 0$ in normalized $\alpha - \beta$ plane for several values of the source frequency σ_0. Point P, of coordinates $(\alpha, \beta, \sigma_0) = (-\frac{1}{4}, 0, \frac{1}{4})$, is the critical resonant point.

The curves represent waves generated by a source travelling to the left wih speed v, and the arrows are normal directions at the points of inflexion. (Adapted from Lighthill [7].)

https://doi.org/10.1017/S033427000000391X Published online by Cambridge University Press

It should be pointed out that the solution which satisfies the radiation condition is that representing waves found in the direction pointing towards the curve $G(\alpha, \beta, \sigma_0 + \delta) = 0$, where $\delta > 0$. Note also that the result in (9) is not valid at points of G where $\kappa = 0$, corresponding to caustics, and near the critical point P.

Also relevant is the group velocity $\mathbf{c}_g$, which is determined by

$$\mathbf{c}_g/v = -\nabla G/G_\sigma,$$

whence it may be shown that, as is to be expected,

$$\mathbf{c}_g/v = \mathbf{k}/2k^{3/2} - (1,0),$$

where $\mathbf{k} = (\alpha, \beta)$, *cf.* Courant and Hilbert [3].

3. Behaviour of $G(\alpha, \beta, \sigma_0)$ near P

We first study the behaviour of the wavenumber curve near the critical point by assuming that

$$\sigma_0 = \tfrac{1}{4} + \varepsilon \quad \text{where } |\varepsilon| \ll 1. \tag{13}$$

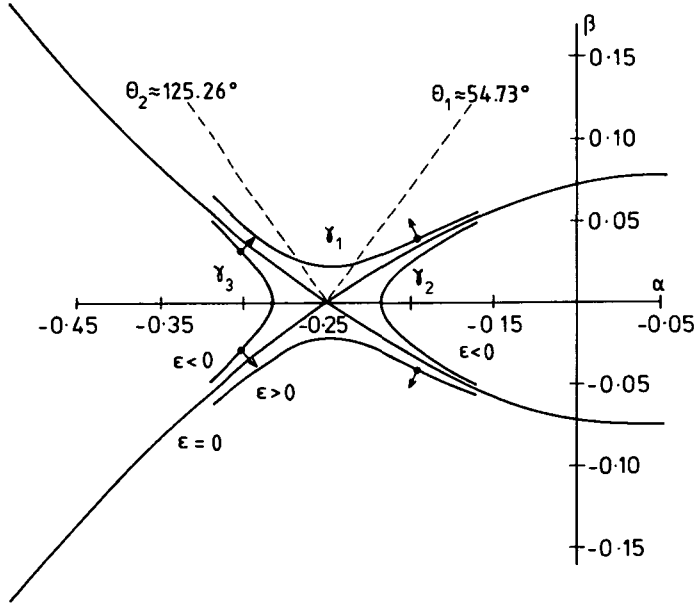

Figure 3. Wavenumber curve $G = 0$ near the critical point P for three values of ε, ($\varepsilon = -10^{-3}$, $\varepsilon = 0.0$ and $\varepsilon = 10^{-3}$). The arrows are the normals to the curve at the inflexion points, pointing in the direction of increasing ε. Also shown are the directions $\theta_1 = \tan^{-1} 2^{1/2}$ and $\theta_2 = \pi - \tan^{-1} 2^{1/2}$, normal to G at the critical point.

https://doi.org/10.1017/S033427000000391X Published online by Cambridge University Press

TABLE 2. Wavenumber curve $G = 0$ near the critical point P for $\varepsilon = 10^{-7}$. θ is the angle of the normal to the curve at the given point and κ is the curvature.

θ	α	β	κ
60^0	−0.2504	0.0004	300.0
70^0	−0.2502	0.0003	1174.0
90^0	−0.2500	0.0002	2240.0
110^0	−0.2498	0.0002	1165.2
120^0	−0.2495	0.0004	270.0
124^0	−0.2489	0.0007	28.5

Figure 3 shows the curve (8) for three values of ε, including $\varepsilon = 0$, and Table 2 gives the curvature for various values of the angle θ of the normal, for $\varepsilon = 10^{-7}$. The table corresponds to the normals to arc γ_1 of Figure 3. However, a similar behaviour is also observed for $\varepsilon < 0$, on arcs γ_2 and γ_3 of the same figure. Since we are considering small values of ε, $\alpha + \frac{1}{4}$ and β are $O(\varepsilon^\nu)$ near the critical point, where $\nu > 0$. It should be pointed out then, that since the asymptotic expansion (9) is valid only if $\alpha_m x + \beta_m y \gg 1$, we must ensure that $|\varepsilon|^\nu r \gg 1$.

Expanding the wavenumber curve (8) in powers of ε, yields

$$G = \beta^2 - \tfrac{1}{2}\xi^2 + 2\xi^3 - \xi^4 + \left(-\tfrac{1}{2} + 3\xi - 6\xi^2 + 4\xi^3\right)\varepsilon + O(\varepsilon^2), \qquad (14)$$

where

$$\xi = \alpha + \tfrac{1}{4}, \qquad (15)$$

and retaining only terms of order ε, it may be deduced that the approximation to G for which ξ, β are small is given by

$$G_1(\xi, \beta) = \beta^2 - \tfrac{1}{2}\xi^2 - \tfrac{1}{2}\varepsilon, \qquad (16)$$

whose constant value contours are hyperbolae in the $\xi - \beta$ plane. A consequence is that ξ, β are $O(\varepsilon^{1/2})$ as $\varepsilon \to 0$.

4. Behaviour of $\eta(x, y, t)$ near P

Consider the hyperbola approximation (16) and assume that (ξ_m, β_m) is a point on $G_1 = 0$. Let θ_0 be the direction normal to G_1 at that point and suppose we approach P by letting $\varepsilon \to 0$ in such a way that θ_0 remains constant, that is, by observing waves at a fixed direction from the source. This direction must be parallel to the gradient of G_1 at (ξ_m, β_m), which is given by

$$(\nabla G_1)_m = (\partial G_1/\partial\xi, \partial G_1/\partial\beta) = (-\xi_m, 2\beta_m), \qquad (17)$$

and therefore

$$-2\beta_m/\xi_m = \tan\theta_0, \qquad (18)$$

https://doi.org/10.1017/S033427000000391X Published online by Cambridge University Press

which is the condition for (ξ_m, β_m) to be the point of stationary phase corresponding to the direction θ_0.

Using (16) and (18), the condition that $G_1(\xi_m, \beta_m) = 0$ yields

$$\xi_m^2 = -\varepsilon \cos^2 \theta_0 / a^2, \tag{19}$$

where

$$a = \left(\cos^2 \theta_0 - \tfrac{1}{2} \sin^2 \theta_0\right)^{1/2}. \tag{20}$$

Note that since ξ_m must be real, if $\varepsilon > 0$, then $|\tan \theta_0| > 2^{1/2}$, and if $\varepsilon < 0$, then $|\tan \theta_0| < 2^{1/2}$.

Substitution of (11), (12), (13) and (19) into (9) gives the result

$$\eta \sim -\frac{ip_0 |\varepsilon|^{-1/4}}{8\rho g} (\pi |a| r)^{-1/2} \exp\left[-\tfrac{1}{4} i(x + t - \pi \operatorname{sgn} \kappa)\right], \tag{21}$$

for fixed r, as $\varepsilon \to 0$, provided $|\varepsilon|^{1/2} r \gg 1$.

Equation (21) is not valid when $a = 0$, that is, along the lines

$$\theta_1 = \tan^{-1} 2^{1/2} \approx 54.73^0, \qquad \theta_2 = \pi - \tan^{-1} 2^{1/2} \approx 125.26^0, \tag{22}$$

which are the normals to $G = 0$ at P as shown in Figure 3. Hence, we assume that $\tan \theta_0 = 2^{1/2}$ and take the approximation

$$G_2(\xi, \beta) = \beta^2 - \tfrac{1}{2}\xi^2 + 2\xi^3 - \tfrac{1}{2}\varepsilon = 0. \tag{23}$$

In this case $(\nabla G_2)_m = (-\xi_m + 6\xi_m^2, 2\beta_m)$. The condition that ∇G_2 is parallel to θ_0 becomes $2\beta_m / (-\xi_m + 6\xi_m^2) = 2^{1/2}$, and the fact that $G_2(\xi_m, \beta_m) = 0$ gives

$$\xi_m = -\tfrac{1}{2}\varepsilon^{1/3}, \tag{24}$$

to lowest order in ε.

Substituting into (9) yields the result that in the directions θ_1, θ_2,

$$\eta \sim -\frac{ip_0 3^{-1/4} |\varepsilon|^{-1/3}}{8\rho g} (\pi r)^{-1/2} \exp\left[-\frac{i}{4}(x + t - \pi \operatorname{sgn} \kappa)\right], \tag{25}$$

for fixed r, as $\varepsilon \to 0$ and provided $|\varepsilon|^{1/3} r \gg 1$.

The asymptotic results in (21) and (25) imply that, given r, the wave amplitude increases as ε decreases. This fact is confirmed numerically in Tables 3 and 4 which give the amplitude $|\eta|$ from (9) in units of $p_0/\rho g$, computed using the exact form of G given in (8). In both tables, the wave amplitude is calculated at a distance

$$r = d / \sin \theta, \tag{26}$$

where d is the non-dimensional distance between the centre of the storm and a point on a coastline which is parallel to the direction of propagation of the storm.

https://doi.org/10.1017/S033427000000391X Published online by Cambridge University Press

TABLE 3. Normalized wave amplitude $10^3 \times |\eta|/(p_0/\rho g)$, from equation (9) for $\varepsilon > 0$. θ is the angle of the normal to the arc γ_1 of the wavenumber curve in Figure 3. Note specially the large amplitudes for θ near $\theta_1 \approx 54.73^0$. Blank spaces correspond to values of θ beyond the inflexion point where (9) does not apply.

ε \ θ	50^0	55^0	60^0	70^0	90^0	100^0	110^0	120^0
10^{-2}	0.46	0.41	0.38	0.34	0.23			
10^{-3}	0.74	0.70	0.64	0.57	0.52	0.53	0.58	
10^{-4}	1.11	1.31	1.15	0.98	0.92	0.93	1.00	1.80
10^{-5}	1.29	2.64	2.06	1.74	1.50	1.68	1.90	2.31
10^{-6}	1.30	5.39	3.80	3.12	2.92	3.00	3.10	3.80
10^{-7}	1.31	11.14	6.80	5.60	5.13	5.27	5.40	6.95

TABLE 4. Normalized wave amplitude $10^3 |\eta|/(p_0/\rho g)$ for $\varepsilon < 0$. (a) Waves normal to arc γ_2 of Figure 3. Note the large amplitudes which occur for θ near $\theta_2 \approx 125.26^0$.

ε \ θ	115^0	120^0	125^0	130^0	135^0	140^0	145^0	150^0
-10^{-2}	0.08	0.09	0.10	0.11	0.10	0.10	0.09	0.09
-10^{-3}	0.23	0.32	0.37	0.38	0.36	0.33	0.30	0.27
-10^{-4}	0.31	0.63	0.98	0.92	0.80	0.72	0.65	0.52
-10^{-5}	0.32	0.74	2.28	1.74	1.50	1.42	1.22	1.12
-10^{-6}	0.33	0.78	5.06	3.75	2.88	2.48	2.18	1 93
-10^{-7}	0.34	0.79	10.53	6.40	5.17	4.36	3.91	3.40

(b) Waves normal to arc γ_3 of Figure 3. Blank spaces correspond to values of θ beyond the inflexion point.

ε \ θ	15^0	20^0	25^0	30^0	35^0	40^0	45^0	50^0
-10^{-2}	0.22	0.27	0.33	0.44	0.65			
-10^{-3}	0.26	0.33	0.38	0.46	0.51	0.64		
-10^{-4}	0.40	0.47	0.55	0.65	0.75	0.87	1.08	
-10^{-5}	0.70	0.86	0.99	1.12	1.27	1.46	1.72	2.29
-10^{-6}	1.22	1.51	1.74	1.95	2.23	2.54	2.96	3.77
-10^{-7}	2.30	2.70	3.00	3.48	3.97	4.45	5.22	6.59

5. The caustic solution

Equation (9) is not valid at points of inflexion of the wavenumber curve, because $\kappa = 0$. However, the method of stationary phase may be extended to yield a more general asymptotic solution in terms of Airy functions which is valid at the point of inflexion and near it (Lighthill [7, Chapter 4]). This is known as the caustic solution and has the property that on one side of it, the waves decay exponentially and on the other side, oscillatory waves are possible. In between, the amplitude reaches a maximum value, determined by the Airy function $\mathrm{Ai}(\zeta)$ (see Figure 5).

https://doi.org/10.1017/S033427000000391X Published online by Cambridge University Press

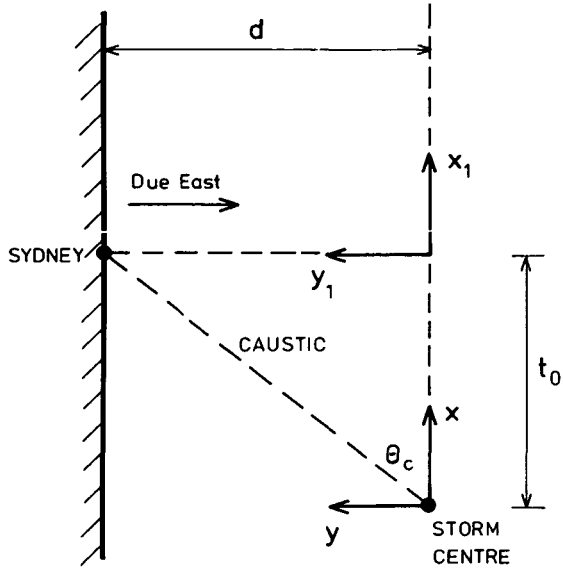

Figure 4. The moving and stationary frames $x - y$ and $x_1 - y_1$ respectively. d is the distance between the centre of the storm and shore and t_0 is the time taken by the caustic to reach the observer after the storm was due East of Sydney.

In fact, it may be shown that

$$\eta \sim \psi(x, y, t)\exp\left[i(\alpha_c x + \beta_c y - \sigma_0 t + \pi/2)\right], \tag{27}$$

as $r \to \infty$, where

$$\psi(x, y, t) = \frac{p_0\left(\alpha_c^2 + \beta_c^2\right)^{1/2}}{\rho g(G_{\bar{\alpha}})_c\left[\frac{1}{2}X(d^3\bar{\alpha}/d\bar{\beta}^3)_c\right]^{1/3}}\mathrm{Ai}\left\{\frac{Y}{\left[\frac{1}{2}X(d^3\bar{\alpha}/d\bar{\beta}^3)_c\right]^{1/3}}\right\}, \tag{28}$$

(α_c, β_c) is an inflexion point of $G = 0$, $\bar{\alpha}$, $\bar{\beta}$ are given in (10) and where

$$X = x\cos\theta_c + y\sin\theta_c, \qquad Y = -x\sin\theta_c + y\cos\theta_c, \tag{29}$$

are the new coordinates in the transformed (x, y) plane and θ_c is the normal direction at the inflexion point. As before, from the two possible directions, we must take the one pointing in the direction of increasing σ_0 as shown by the arrows of Figures 2 and 3.

It is important to note that both equations (9) and (27) represent waves as seen from the moving frame which is travelling with the source. In order to compare the theory with observations of waves generated by cyclone Pam, we must refer the equations to coordinates (x_1, y_1) fixed with respect to the shore. Figure 4 depicts a typical situation when a caustic making an angle θ_c reaches Sydney.

https://doi.org/10.1017/S033427000000391X Published online by Cambridge University Press

TABLE 5. Maximum amplitude $10^3 \times \psi$ in units of $p_0/\rho g$, for several values of ε, (a) $\varepsilon > 0$, (b) $\varepsilon < 0$. α_c is the value of α at the inflexion point and θ_c is the normal to $G = 0$ at such point. T_c' denotes the observed period and t_0' the time computed from equation (30). Primes denote the corresponding dimensional quantities as defined in (1).

(a) $\varepsilon > 0$.

ε	α_c	Maximum wave Amplitude	Direction of caustic θ_c	Wave period T_c' (Sec)	Time t_0' (Hrs)
10^{-2}	−0.153	1.10	99.12^0	8.61	−5.21
10^{-3}	−0.196	2.28	114.10^0	7.96	−14.53
10^{-4}	−0.223	4.45	120.32^0	7.53	−18.99
10^{-5}	−0.237	8.07	123.02^0	7.31	−21.10
10^{-6}	−0.244	14.07	124.23^0	7.21	−22.04
10^{-7}	−0.247	24.06	124.79^0	7.16	−22.56
10^{-8}	−0.248	40.54	125.04^0	7.14	−22.77
0.0	−0.250	∞	$\theta_2 \approx 125.26^0$	7.12	−23.00

(b) $\varepsilon < 0$.

ε	α_c	Maximum wave Amplitude	Direction of caustic θ_c	Wave period T_c' (Sec)	Time t_0' (Hrs)
-10^{-2}	−0.439	4.45	36.97^0	5.25	43.14
-10^{-3}	−0.323	4.59	45.48^0	6.22	31.94
-10^{-4}	−0.281	6.19	50.20^0	6.70	27.05
-10^{-5}	−0.264	9.40	52.58^0	6.93	24.84
-10^{-6}	−0.256	15.03	53.72^0	7.03	23.83
-10^{-7}	−0.253	24.59	54.26^0	7.08	23.36
-10^{-8}	−0.251	40.65	54.52^0	7.10	23.15
0.0	−0.250	∞	$\theta_1 \approx 54.73^0$	7.12	23.00

From the diagram, the time taken by the caustic to reach the observer after the storm was due East of Sydney is

$$t_0 = d/\tan\theta_c, \tag{30}$$

where d is defined in (26).

The normalized wave frequency σ_r measured by the observer is given by the Doppler relationship $\sigma_r = \sigma_0 - \alpha_c$, where α_c is the value of α at the inflexion point. The observed period then becomes

$$T_c = 2\pi/(\sigma_0 - \alpha_c). \tag{31}$$

Tables 5(a) and 5(b) give the maximum amplitude of the caustic solution (27), which corresponds to the maximum of ψ in Figure 5, for various values of ε. The

https://doi.org/10.1017/S033427000000391X Published online by Cambridge University Press

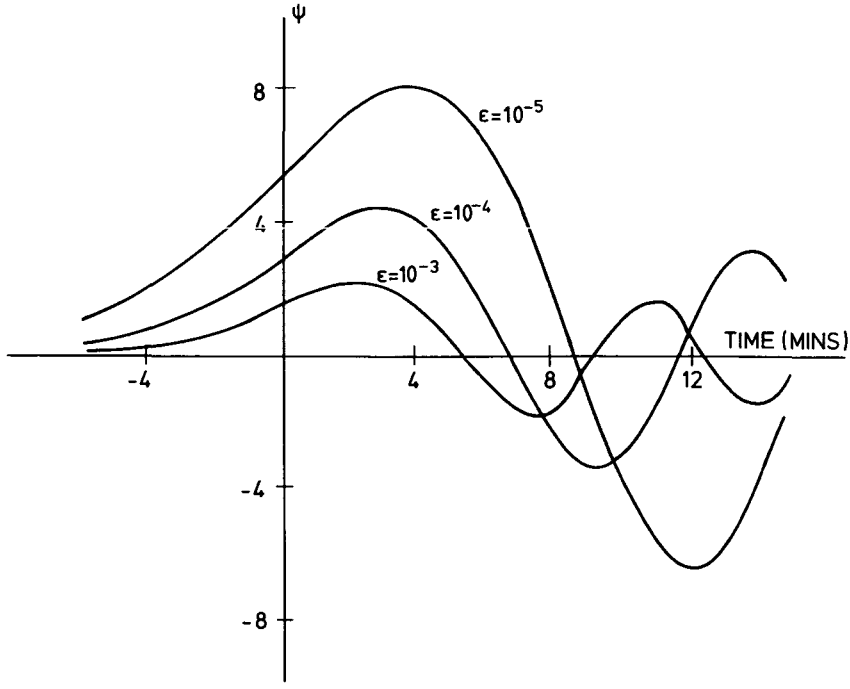

Figure 5. The relative amplitude of the Airy envelope $10^3 \times \psi$ in (28) in units of $p_0/\rho g$ as a function of time, for three values of ε. The abcissa refers to the time taken for the envelope to pass an observer in Sydney, the origin being at the time t_0' given for corresponding values of ε in Table 5a.

fourth column gives the direction θ_c of the normal to G at the inflexion point and shows that the limiting values as $\varepsilon \to 0$, are θ_1 and θ_2 as defined in (22).

The next column gives the wave period as computed from (31). The last column shows the time taken by the caustic to reach the observer as calculated from equation (30). The negative times in Table 5(a) mean that waves reach the observer before the storm is due east of Sydney. We must point out that the dimensional quantities, denoted by primes, correspond to a storm speed $v = 20$ km/h and a distance of 650 km from the shore.

In order to compare the relative magnitude of the waves generated by the caustics as they approach the observer, we substitute $x = t - t_0$ and $y = d$ in equation (29) and then plot the amplitude as a function of the time t. Figure 5 shows the function ψ in units of $p_0/\rho g$ for three values of ε. Note that one of the effects of varying ε, is to change the angle θ_c which in turn changes the value of t_0 as seen in Table 5. For simplicity, however, the three curves are plotted with respect to the same time origin.

https://doi.org/10.1017/S033427000000391X Published online by Cambridge University Press

The fact that $|\eta| \to \infty$ when ε decreases, as Table 5 shows, may be proved analytically by means of an expansion similar to (21). Assuming that θ_c is the normal direction at a point of inflexion (ξ_c, β_c) of $G = 0$, equations (18) and (19) now become

$$\beta_c = -\tfrac{1}{2}\xi_c \tan\theta_c, \qquad \xi_c^2 = -\varepsilon \cos^2\theta_c / a^2. \tag{32}$$

Using the result

$$d^3\bar{\alpha}/d\bar{\beta}^3 = G_{\bar{\alpha}}^{-2}\left(3G_{\bar{\alpha}\bar{\beta}}G_{\bar{\beta}\bar{\beta}} - G_{\bar{\alpha}}G_{\bar{\beta}\bar{\beta}\bar{\beta}}\right) \tag{33}$$

where $(\bar{\alpha}, \bar{\beta})$ are given in (10) and $\alpha = \xi - \frac{1}{4}$, yields

$$\eta \sim -\frac{ip_0 \mathrm{Ai}(0)\,|\varepsilon|^{-1/6}}{4\rho g}\left[\frac{\frac{1}{9}\tan^2\theta_c \operatorname{cosec}^3\theta_c}{X\left(1+\tan^2\theta_c\right)^{1/2}}\right]^{1/3} \exp\left[i(\alpha_c x + \beta_c y - \sigma_0 t)\right], \tag{34}$$

as $\varepsilon \to 0$, provided $|\varepsilon|^{1/2} r \gg 1$, where $\mathrm{Ai}(0) = 3^{-2/3}\Gamma(2/3) \approx 0.355$, and

$$a = \left(\cos^2\theta_c - \tfrac{1}{2}\sin^2\theta_c\right)^{1/2}.$$

6. A uniform asymptotic expansion for $\eta(x, y, t)$

The asymptotic expressions calculated in Section 4 assume that $r \gg 1$, and prove to be not uniformly valid as $\varepsilon \to 0$. In order to investigate more closely the solution near the critical point, we need an expansion for η which is valid for fixed r, as $\varepsilon \to 0$ and it is assumed that r is large compared with the dimensions of the storm centre. However, the exact wavenumber curve is too complicated to allow such an expansion to be obtained. Hence, to the first order in ε, we replace G by G_1 given in (16). The curve $G_1 = 0$ is a hyperbola with asymptotes $\xi^2 = 2\beta^2$.

It is important to point out that this approximation takes into account the large curvature of G near P and therefore it will be useful in the study of the effect the large curvature has on the directions of the observed waves. Note that for small $|\varepsilon|$ the large curvature ensures that the small portion of the curve $G = 0$ near P gives rise to arcs of wave directions, in the wedge illustrated in Figure 6a for $\varepsilon > 0$, and Figure 6b for $\varepsilon < 0$.

The limitations of the approach in this section is that the hyperbolae $G_1 = 0$ do not have inflexion points, so that the contributions from caustics cannot be included. Moreover, the asymptotes of $G_1 = 0$ give rise to singularities which do not have a counterpart in $G = 0$. Nevertheless, away from the asymptotes, a useful uniform approximation is obtained as follows.

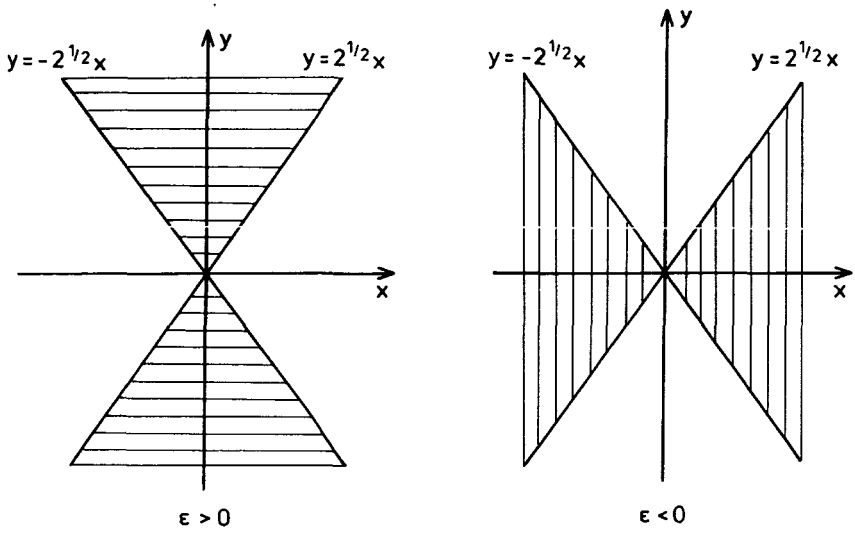

Figure 6. Regions of the $x - y$ plane where equation (35) represents non-decaying waves propagating away from the source, for positive and negative ε. The $x - y$ frame is fixed with respect to the source, which is travelling to the left.

It is shown in the Appendix that, with the approximation to G given in (16), the surface displacement is given by

$$\eta = -\frac{p_0 \operatorname{sgn} y}{2^{3/2}\pi\rho g}\left[AK_0(a\varepsilon^{1/2}r) + BK_1(a\varepsilon^{1/2}r)\right]\exp\left\{-i\left[\tfrac{1}{4}x + t\left(\varepsilon + \tfrac{1}{4}\right)\right]\right\} \quad (35)$$

where a is given in (20),

$$A = i\left(\tfrac{1}{4} + \varepsilon a^2\cos^2\theta + \tfrac{1}{2}\varepsilon\right), \qquad B = a\varepsilon^{1/2}\cos\theta(1 - i\cos\theta/r + \varepsilon), \quad (36)$$

$K_0(\zeta)$ and $K_1(\zeta)$ being the modified Bessel functions of the second kind.

It may be shown that (*e.g.* Abramowitz and Stegun [1, page 378]),

$$K_i(\zeta) \sim (\pi/2\zeta)^{1/2}\exp(-\zeta), \qquad |\zeta| \to \infty, i = 1, 2.$$

Hence, equation (35) results in non-decaying waves propagating away from the source only if the argument of the Bessel functions is imaginary. If $\varepsilon > 0$, this occurs when $|\tan\theta| > 2^{1/2}$, if $\varepsilon < 0$, when $|\tan\theta| < 2^{1/2}$. This relationship between ε and $\tan\theta$ has already been found from an examination of equation (19). However, from (35), we conclude that waves with wavenumber and frequency near the critical point are observed from the source, in all directions within the corresponding wedges shown in Figure 6.

Further, using the results

$$K_0(\zeta) \sim -\ln\zeta, \qquad K_1(\zeta) \sim \zeta^{-1} \quad \text{as } \zeta \to 0,$$

https://doi.org/10.1017/S033427000000391X Published online by Cambridge University Press

we obtain, for fixed r and $a \neq 0$,

$$\eta(x, y, t) \sim \frac{p_0 \operatorname{sgn} y}{2^{3/2}\pi\rho g}\left(\frac{i}{8}\right)\ln|\varepsilon|, \tag{37}$$

as $\varepsilon \to 0$. This result is uniformly valid as $\varepsilon \to 0$, and there are no restrictions on the relative magnitudes of r and ε. Note that (37) represents a weaker singularity as $\varepsilon \to 0$, than that predicted by (21).

Similarly, for fixed r and $\varepsilon \neq 0$,

$$\eta(x, y, t) \sim \frac{p_0 \operatorname{sgn} y}{2^{3/2}\pi\rho g}\left(\frac{i}{4}\right)\ln|a|, \tag{38}$$

for $|a| \ll 1$. This result, however, is not valid in the neighbourhood of $a = 0$, since, in this representation, the approximate curve has asymptotes, the presence of which affect the approximation accuracy.

7. Discussion

Cyclone Pam travelled at an estimated speed v of 20 km/h at an approximate distance of 650 km from shore. The calculated source period of waves generated at the critical point $(\alpha, \beta, \sigma_0) = (-\frac{1}{4}, 0, \frac{1}{4})$ is about 14 seconds and the corresponding Doppler shifted period to an observer at rest is (*cf.* equation (31))

$$T' = 2\pi v/g(\sigma_0 - \alpha) = 7.12 \text{ sec.} \tag{39}$$

The computed periods of waves generated by the caustics near the critical point, as given in Table 5, are also about 7 seconds. These values are very close to the actual observed periods in Table 1.

Suppose, now, that the centre of the storm generates waves whose frequency spectrum is concentrated near the critical value and consider the following two cases, (a) waves near θ_1, and (b) waves near θ_2.

Case (a)–Referring to Figure 3, for values of the frequency for which $\varepsilon > 0$, we expect to see waves whose directions are normal to arc γ_1 of the wavenumber curve $G = 0$. In particular, relatively large waves will be observed along a direction θ near θ_1, as predicted in Table 3. We then add the contributions of the large waves generated by the caustic with inflexion point lying on arc γ_3, corresponding to $\varepsilon < 0$. This caustic also points towards $\theta \approx \theta_1$ as shown in Table 5(b).

https://doi.org/10.1017/S033427000000391X Published online by Cambridge University Press

Case (b)–Sections of the spectrum for which $\varepsilon < 0$, give rise to waves normal to arc γ_2 (waves ahead of the storm) and where large amplitudes occur for θ near θ_2. Waves generated by the caustic with inflexion point on arc γ_1, also point towards a direction close to the value of θ_2 as given in Table 5a.

This shows that waves of relatively large amplitudes will be observed along directions given by the lines θ_1 and θ_2. Moreover, if ε is sufficiently small, then equation (35) applies and very large waves are expected in all directions within the wedges of Figure 6, (6(a) for $\varepsilon > 0$ and 6(b) for $\varepsilon < 0$). However, it should be noted that waves within the wedge of Figure 6(a) travel a much shorter distance to shore than the corresponding waves within the other wedge. Hence, we expect the former waves to have larger amplitudes than the latter, by the time they reach the observer.

To summarize, the theory predicts that once a steady state regime has been established very large waves will first be observed when line θ_2 reaches the observer. The position of the cyclone when this occurs is represented by point B_1 in Figure 7. Relatively large waves will then be observed for 45.5 hrs, corresponding to waves within the wedge of Figure 6(a). Finally, when the storm is at point B_2, line θ_1 reaches the observer and after that, the amplitude starts to decrease.

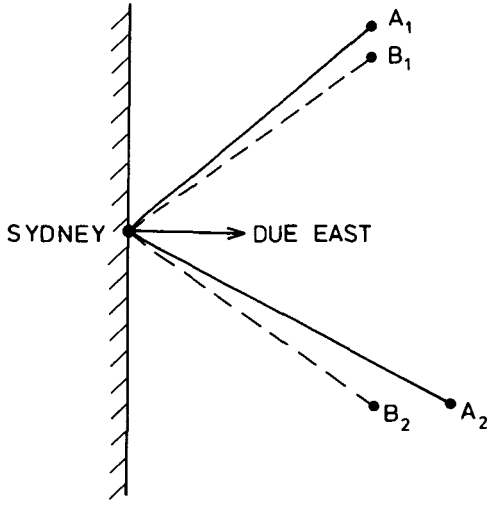

Figure 7. Points A_1 and A_2 represent the estimated positions of the storm centre with respect to Sydney on days 37 and 39. Point A_1 shows when relatively large waves were first observed at approximately 5 *a.m.* on day 37. After the cyclone reached A_2 (6 *p.m.*, day 39), the wave amplitude began to decrease.

Points B_1 and B_2 represent the position of the point source model. Line θ_2 reaches Sydney when the source is at B_1, and line θ_1 reaches Sydney when it is at point B_2. The cyclone is estimated to be due East of Sydney at 2 *a.m.* on day 38.

The observations of waves from cyclone Pam give the following results. From Table 1, large waves were first observed between 5 *a.m.* and 3 *p.m.* on day 37, and they would correspond to the arrival of line θ_1. Point A_1 in Figure 7 shows the estimated position of the storm when this occurs, taken from the isobars in Figure 1 (estimated value of $\theta \approx 130^0$). Relatively large waves were then observed for about two days, until approximately 6 *p.m.* on day 39 (point A_2, $\theta \approx 60^0$, Figure 7).

The arrival of the large waves predicted by the theory along the line θ_1 is not evident from the data in Table 1. More refined measurements would be needed to be able to observe the large waves along this particular direction. The wave amplitude, however, starts to decrease after point A_2, as we expect from the discussion in the summary above.

There is therefore some agreement with observations and hence the oscillatory point source used to represent the cyclone has proved useful and not too unrealistic. However, the infinite amplitudes predicted by (37), show that the linearized model breaks down at $\varepsilon = 0$ and non-linear terms should be included in the governing equations to obtain a more accurate description of the behaviour at the critical point.

The amplitudes given in (25) and (38) on the other hand, show that the linearized wave equations predict infinite amplitudes in the directions θ_1 and θ_2 unless some damping mechanism is included in the original equations. More realistically, an initial value problem may be considered, with the pressure source being switched-on at some finite value of time. This problem and the effect of a continuous spectrum are the subject of current investigations, and these will have a bearing on the interpretation of the results in this paper.

Now that microwave and radar observations of swell are possible for large areas of ocean, the results in this paper suggest the swell patterns which would be observed by satellite from a travelling cyclone. It would be interesting to see whether the effects of circular asymmetry and Earth's rotation are sufficiently significant to require recognition in the theory.

Appendix

Applying the Fourier transform (6) to (2), (3) and (4) with (5) and solving for the velocity potential ϕ, one obtains in place of (7),

$$\phi(x, y, t) = -\frac{ip_0 e^{-i\sigma_0 t}}{4\pi^2 \rho g} \int_{-\infty}^{\infty} \int_{-\infty}^{\infty} \frac{(\alpha - \sigma_0) e^{i(\alpha x + \beta y)} d\beta \, d\alpha}{G(\alpha, \beta, \sigma_0)}, \qquad (A.1)$$

where $\sigma_0 = \frac{1}{4} + \varepsilon$ and $G(\alpha, \beta, \sigma_0)$ is given in (8).

https://doi.org/10.1017/S033427000000391X Published online by Cambridge University Press

Replacing $G(\alpha, \beta, \sigma_0)$ by the hyperbola (16), the change of variables $\xi = \alpha + \frac{1}{4}$ yields

$$\phi(x, y, t) = -\frac{ip_0 \exp\{-i[\frac{1}{4}x + (\varepsilon + \frac{1}{4})t]\}}{8\pi^2 \rho g} \int_{-\infty}^{\infty} \int_{-\infty}^{\infty} \frac{(\xi - \frac{1}{2}) e^{i(\xi x + \beta y)} d\beta \, d\xi}{G_1(\xi, \beta, \varepsilon)}, \tag{A.2}$$

where $G_1(\xi, \beta, \varepsilon) = \beta^2 - \frac{1}{2}(\xi^2 + \varepsilon)$. The integral with respect to β in (A.2) is now evaluated using contour integration by deforming the path into a semicircle in the upper half plane if $y > 0$ and in the lower half plane if $y < 0$. The integrand has two poles at $\beta = \pm\beta_0$, where

$$\beta_0 = 2^{-1/2}(\xi^2 + \varepsilon)^{1/2}. \tag{A.3}$$

In order to satisfy the radiation condition, we replace ε by $\varepsilon + i\varepsilon_1$, $(\varepsilon_1 > 0)$ and then let ε_1 tend to zero. For small ε_1 the approximate position of the poles in the complex β-plane is given by

$$\beta_0 = 2^{-1/2}(\xi^2 + \varepsilon)^{1/2} + \frac{i\varepsilon_1}{2^{3/2}(\xi^2 + \varepsilon)^{1/2}} + O(\varepsilon_1^2).$$

Jordan's lemma and residue theory then yield

$$\phi(x, y, t) = \frac{2^{1/2} p_0 \operatorname{sgn} y}{8\pi\rho g} (\psi_1 + \psi_2) \exp\{-i[\tfrac{1}{4}x + (\varepsilon + \tfrac{1}{4})t]\}, \tag{A.4}$$

where

$$\psi_1 = -\frac{1}{2} \int_{-\infty}^{\infty} \frac{\exp[i|y| 2^{-1/2}(\xi^2 + \varepsilon)^{1/2} + i\xi x] d\xi}{(\xi^2 + \varepsilon)^{1/2}}, \tag{A.5}$$

and

$$\psi_2 = \int_{-\infty}^{\infty} \frac{\xi \exp[i|y| 2^{-1/2}(\xi^2 + \varepsilon)^{1/2} + i\xi x] d\xi}{(\xi^2 + \varepsilon)^{1/2}}. \tag{A.6}$$

From a table of Fourier integrals (*e.g.* Campbell and Foster [2, page 111]) one obtains

$$\psi_1 = 2K_0(a\varepsilon^{1/2} r). \tag{A.7}$$

Differentiating (A.7) with respect to x and using the relation $K_0'(\zeta) = -K_1(\zeta)$ gives

$$\psi_2 = 2i \cos\theta \, a\varepsilon^{1/2} K_1(a\varepsilon^{1/2} r), \tag{A.8}$$

https://doi.org/10.1017/S033427000000391X Published online by Cambridge University Press

where

$$a = \left(\cos^2\theta - \tfrac{1}{2}\sin^2\theta\right)^{1/2}.$$

Finally, substitution of (A.4) into (3) gives (35).

References

[1] M. Abramowitz and I. A. Stegun (eds.), *Handbook of mathematical functions* (Dover, New York, 1965).

[2] G. A. Campbell and R. M. Foster, *Fourier integrals for practical applications* (Van Nostrand, Princeton, 1948).

[3] R. Courant and D. Hilbert, *Methods of mathematical physics*, *Volume* 2 (Interscience, New York, 1953).

[4] G. D. Crapper, "Surface waves generated by a travelling pressure point", *Proc. Roy. Soc. London Ser. A* 282 (1964), 547–558.

[5] M. J. Lighthill, "Studies on magneto-hydrodynamic waves and other anisotropic wave motions", *Phil. Trans. Roy. Soc. London Ser. A* 252 (1960), 397–430.

[6] M. J. Lighthill, "On waves generated in dispersive systems by travelling forcing effects, with applications to the dynamics of rotating fluids", *J. Fluid Mech.* 27 (1967), 725–752.

[7] M. J. Lighthill, *Waves in fluids* (Cambridge University Press, 1978).